

PAPER

Discovery of Two Families of Vsb-Based Compounds with V-Kagome Lattice

To cite this article: Yuxin Yang *et al* 2021 *Chinese Phys. Lett.* **38** 127102

View the [article online](#) for updates and enhancements.

You may also like

- [Signatures of a hybridization gap in magnetic susceptibility of \$Ce_{1-x}La_xOs_4Sb_{4-x}\$](#)
B Andraka, A Ross and C R Rotundu
- [The effect of \$Cu_2O\$ nanoparticle dispersion on the thermoelectric properties of n-type skutterudites](#)
M Battabyal, B Priyadarshini, D Sivaprahasam et al.
- [Synthesis and thermoelectric properties of Nd-single filled p-type skutterudites](#)
Hong Wu, , Nusrat Shaheen et al.

Discovery of Two Families of VSb-Based Compounds with V-Kagome Lattice

Yuxin Yang(杨雨欣)^{1,2†}, Wenhui Fan(樊文辉)^{1,2†}, Qinghua Zhang(张庆华)^{1†}, Zhaoxu Chen(陈昭旭)^{1,2}, Xu Chen(陈旭)^{1,2}, Tianping Ying(应天平)^{1*}, Xianxin Wu(吴贤新)³, Xiaofan Yang(杨小帆)⁴, Fanqi Meng(孟繁琦)⁵, Gang Li(李岗)^{1,6}, Shiyan Li(李世燕)⁴, Lin Gu(谷林)^{1,6}, Tian Qian(钱天)^{1,6}, Andreas P. Schnyder³, Jian-gang Guo(郭建刚)^{1,6*}, and Xiaolong Chen(陈小龙)^{1,6*}

¹Beijing National Laboratory for Condensed Matter Physics, Institute of Physics, Chinese Academy of Sciences, Beijing 100190, China

²School of Physical Sciences, University of Chinese Academy of Sciences, Beijing 100049, China

³Max-Planck-Institut für Festkörperforschung, Heisenbergstrasse 1, D-70569 Stuttgart, Germany

⁴State Key Laboratory of Surface Physics, Department of Physics, Fudan University, Shanghai 200438, China

⁵School of Materials, Tsinghua University, Beijing 100084, China

⁶Songshan Lake Materials Laboratory, Dongguan 523808, China

(Received 19 November 2021; accepted 22 November 2021; published online 27 November 2021)

We report the structure and physical properties of two newly discovered compounds AV_8Sb_{12} and AV_6Sb_6 ($A = Cs, Rb$), which have C_2 (space group: $Cmmm$) and C_3 (space group: $R\bar{3}m$) symmetry, respectively. The basic V-kagome unit appears in both compounds, but stacking differently. A V_2Sb_2 layer is sandwiched between two V_3Sb_5 layers in AV_8Sb_{12} , altering the V-kagome lattice and lowering the symmetry of kagome layer from hexagonal to orthorhombic. In AV_6Sb_6 , the building block is a more complex slab made up of two half- V_3Sb_5 layers that are intercalated by Cs cations along the c -axis. Transport property measurements demonstrate that both compounds are nonmagnetic metals, with carrier concentrations at around 10^{21} cm^{-3} . No superconductivity has been observed in CsV_8Sb_{12} above 0.3 K under *in situ* pressure up to 46 GPa. Compared to CsV_3Sb_5 , theoretical calculations and angle-resolved photoemission spectroscopy reveal a quasi-two-dimensional electronic structure in CsV_8Sb_{12} with C_2 symmetry and no van Hove singularities near the Fermi level. Our findings will stimulate more research into V-based kagome quantum materials.

DOI: 10.1088/0256-307X/38/12/127102

The kagome net, a corner-sharing tiling pattern of triangular plaquettes, is a standard model for understanding nontrivial topology, frustrated magnetism, and correlated phenomena. The frustrated lattice geometry endows a wealth of unique physical features to the lately intensely researched kagome metals, including flat bands, van Hove singularity, and topological band crossover. Pure kagome layers, on the other hand, cannot stand alone and are usually intergrown with other building blocks. The stacking-induced interaction and charge donation bring rich varieties to the band structures inherited from the kagome lattice. Prominent examples are noncollinear antiferromagnetism in Mn_3Sn ,^[1] Dirac fermionic in ferromagnetism in Fe_3Sn_2 ,^[2] Chern-gapped Dirac fermion in ferromagnetic $TbMn_6Sn_6$,^[3] and Weyl fermions in the ferromagnet $Co_3Sn_2S_2$.^[4]

The seminal discovery of AV_3Sb_5 ^[5,6] has inspired a new surge of interest. As seen in Fig. 1, the vanadium sublattice forms a perfect kagome net that is interwoven with Sb atoms both within and outside of the plane to build a V_3Sb_5 monolayer. Despite the lack of magnetization, AV_3Sb_5 is dis-

covered to be Z_2 topological materials with alternative ground states such as the charge density wave (CDW) ordering and superconductivity.^[7,8] This CDW ordering is later proved not driven by strong electron-phonon coupling^[9–16] and competes with superconductivity.^[17] Subsequent studies further discovered exciting discoveries including the reentrance of superconductivity under high pressure,^[18–22] the enormous anomalous Hall effect,^[23,24] pair density wave,^[13] and evidence of plausible unconventional superconductivity.^[13,25] Changing the stacking sequence of the kagome layer with different building components and seeing the consequences on physical characteristics is both exciting and practically doable, given the very weak interlayer interactions. However, only partial removal of A element has been realized through selective oxidation of thin flakes, resulting in a shift of van Hove singularity,^[26,27] enhanced T_c ,^[17,28–31] and A-vacancy ordering.^[32] The construction of novel vanadium-based kagome structures by altering the stacking sequence has not been realized so far.

In this Letter, we investigate the possibility of

Supported by the National Key Research and Development Program of China (Grant Nos. 2017YFA0304700 and 2018YFE0202601), the National Natural Science Foundation of China (Grant Nos. 51922105, 51772322, 52025025, and 52072400), and the Beijing Natural Science Foundation (Grant No. Z2000005).

[†]These authors contributed equally to this work.

*Corresponding authors. Email: ying@iphy.ac.cn; jgguo@iphy.ac.cn; xlchen@iphy.ac.cn

© 2021 Chinese Physical Society and IOP Publishing Ltd

constructing novel A–V–Sb compounds by rearranging the constituent layers. As a result, the AV_8Sb_{12} and AV_6Sb_6 (A = Rb, Cs) families of compounds are found. The initial C_6 symmetry is decreased to C_2 and C_3 in AV_8Sb_{12} and AV_6Sb_6 , respectively, by inserting alternative building blocks or changing the stacking sequences. Their band structures and electric conductivity are substantially altered when the symmetry is broken. Theoretical calculations and angle-resolved photoemission spectroscopy (ARPES) measurements reveal previously unseen features compared to those of AV_3Sb_5 .

Experimental—Single Crystal Growth. Single crystals of AV_8Sb_{12} and AV_6Sb_6 (A = Cs, Rb) were grown via the self-flux method. AV_8Sb_{12} (AV_6Sb_6) single crystals were grown by mixing Cs (99.98%), V (powder, 99.99%) and Sb (ingot, 99.999%) with the molar ratio of 1.2:6:15 (1.2:6:18), loaded into an alumina container and then sealed into a silica tube in vacuum. The mixture was subsequently heated to 1373 K and kept for 24 h, then cooled to 1173 K (1273 K) in 72 h. The excess flux was removed by centrifuging at corresponding temperature.

Characterization. The diffraction was performed on a Panalytical X'pert diffractometer with a $Cu K_\alpha$ anode (1.5481 Å). The composition and structure of the sample were determined by the combination of an energy dispersive spectroscope and a scanning transmission electron microscope (STEM). The atomic arrangement of the two phases was observed by a spherical aberration-corrected ARM200F (JEOL, Tokyo, Japan) STEM operated at 200 kV with a convergence angle of 25 mrad and collected angle from 70 to 250 mrad. The high angle annular dark field STEM (HAADF-STEM) image was collected with a dwell time of 10 μ s each pixel. The transport measurement under ambient and high pressure was performed on a Quantum Design physical property measurement system (PPMS). A Keithley 2182A, a Keithley 6221, and a Keithley 2400 were used to measure the transport properties under external magnetic fields. Magnetization measurements were performed using a Quantum Design magnetic properties measurement system (MPMS3). The high-pressure resistivity of CsV_8Sb_{12} samples was measured by a diamond anvil cell (DAC) range from 2 K to 400 K with the van der Pauw method. The resistance experiments were performed using Be–Cu cells. The cubic boron nitride (cBN) powders (200 and 300 nm in diameter) were employed as the medium to transfer pressure. The pressure was calibrated using the ruby fluorescence method at room temperature before and after the measurement.

Angle-Resolved Photoemission Spectroscopy. All the ARPES data shown are recorded at the “Dreamline” beamline of the Shanghai Synchrotron Radiation Facility. The energy and angular resolutions are set to 15 to 25 meV and 0.2°, respectively. All the samples

for ARPES measurements are mounted in a BIP argon (>99.9999%) filled glove box, cleaved *in situ*, and measured at 25 K in a vacuum better than 5×10^{-11} torr.

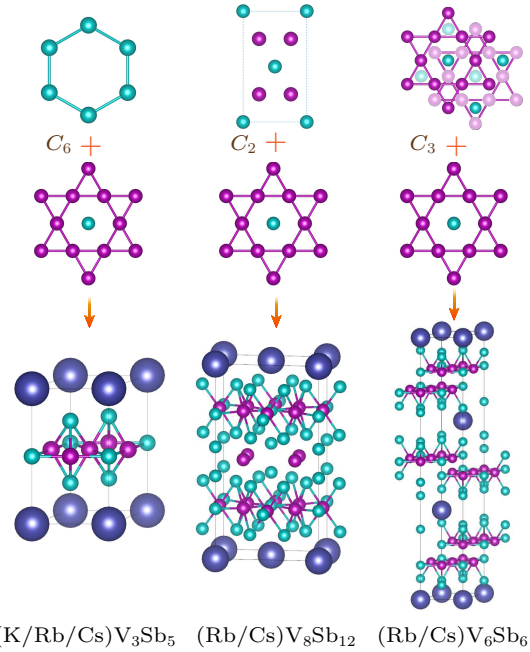


Fig. 1. Crystal structure of AV_3Sb_5 , AV_8Sb_{12} , and AV_6Sb_6 (A = K, Rb, Cs). Blue, violet and green balls are A, V, and Sb atoms, respectively.

Theoretical Calculation. Our DFT calculations employ the projector augmented wave method^[33] encoded in the Vienna *ab initio* simulation package (VASP),^[34] and both the local density approximation and generalized-gradient approximation^[35] for the exchange-correlation functional are used. Throughout this work, the cutoff energy of 500 eV is taken for expanding the wave functions into a plane-wave basis. In the calculation, the Brillouin zone is sampled in the k space within the Monkhorst–Pack scheme.^[36] The number of these k points is $9 \times 9 \times 5$ for the primitive cell. We relax the lattice constants and internal atomic positions, where the plane wave cutoff energy is 600 eV. Forces are minimized to less than 0.01 eV/Å in the relaxation. The obtained lattice constants of CsV_8Sb_{12} are $a = 5.455$ Å, $b = 9.515$ Å and $c = 18.25$ Å, which are in good agreement with the experimental values of $a = 9.516$ Å, $b = 5.451$ Å, and $c = 18.128$ Å.

Results and Discussions. The crystal structures of AV_8Sb_{12} and AV_6Sb_6 are obtained by combining an x-ray diffractometer and an STEM, as shown in Fig. 1, together with the structure of AV_3Sb_5 for comparison. The three A–V–Sb compounds all have a V-based kagome lattice with a centered Sb atom as a common building block. Each V-based kagome layer is sandwiched by two sets of Sb honeycomb lattices in the AV_3Sb_5 , which has a space group of $P6/mmm$ with C_6 symmetry. The crystal structure is rather simple, with the lattice constants of $a = 5.4922$ Å

and $c = 9.8887 \text{ \AA}$. $\text{AV}_8\text{Sb}_{12}$ and AV_6Sb_6 , on the other hand, reveal richer crystal structures due to the intercalation of low symmetric structural units. In $\text{AV}_8\text{Sb}_{12}$, an orthorhombic V_2Sb_2 layer is sandwiched between two V_3Sb_5 units, forming a V_8V_{12} unit. The space group is $Cmmm$ with lattice constants of $a = 5.4510 \text{ \AA}$, $b = 9.5164 \text{ \AA}$, and $c = 18.1282 \text{ \AA}$. The a -axis is approximately $\sqrt{3}$ times that of AV_3Sb_5 . As for AV_6Sb_6 , the basic unit can be viewed as a two- V_3Sb_5 -connected slab by deleting the middle two Sb layers.

Each half- V_3Sb_5 unit is displaced by $(1/2, 1/2, 0)$, and the Cs atoms run down the c -axis to separate the slabs. The space group is $R\bar{3}m$ with $a = 5.3172 \text{ \AA}$ and $c = 34.0741 \text{ \AA}$, in which the c -axis is almost 3 times that of AV_3Sb_5 . $\text{AV}_8\text{Sb}_{12}$ and AV_6Sb_6 can be viewed as derivative phases of the AV_3Sb_5 phase. Since the V-based kagome lattice is mostly intact, exotic properties like superconductivity and charge order are highly expected.

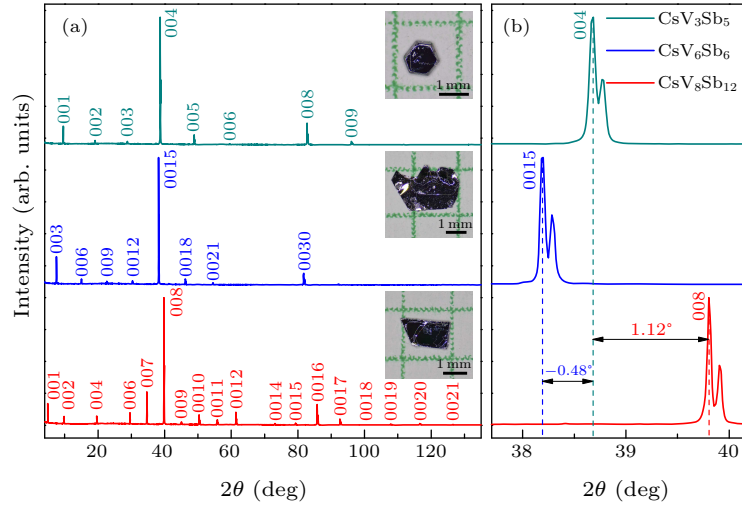


Fig. 2. (a) XRD patterns of CsV_3Sb_5 , $\text{CsV}_8\text{Sb}_{12}$ and CsV_6Sb_6 . (b) The zoomed-in peaks (004), (0015) and (008) from $\sim 38^\circ$ to $\sim 40^\circ$.

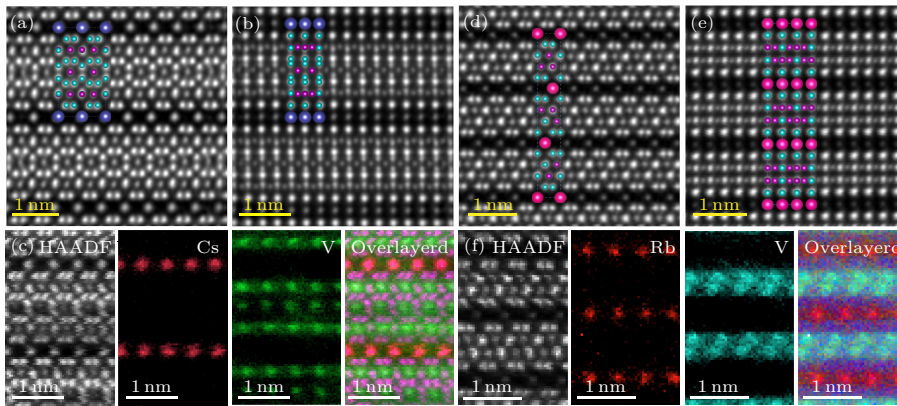


Fig. 3. Atomic structures of $\text{CsV}_8\text{Sb}_{12}$ and RbV_6Sb_6 characterized by STEM. The HAADF image along the [100] (a) and [110] (b) projections, where the structure model is overlaid to show the atomic arrangement. (c) The elemental mapping of $\text{CsV}_8\text{Sb}_{12}$ based on the EELS spectra. The overlaid image is composed of Red Cs, green V, and purple HAADF contrast. The HAADF image along the [100] (d) and [110] (e) projections of RbV_6Sb_6 , where the structure model of RbV_6Sb_6 is overlaid to show the atomic arrangement. (f) The elemental mapping of RbV_6Sb_6 based on the EELS spectra. The overlaid image is composed of Red Rb, green V, and purple HAADF contrast.

We have grown the single crystals of three A–V–Sb compounds [insets of Fig. 2(a)]. All the three samples have a layered structure with metallic luster and a shining surface. From the XRD patterns, we can index the lattice constant c based on the $00l$ peak. The calculated c values in the three compounds agree well with the proposed lattice constants after structural re-

laxation. We further perform atomic resolved STEM imaging and EELS spectra mapping along the two main zone axes: [100] and [110]. The atomic arrangements in each layer can be identified clearly, as shown in Figs. 3(a) and 3(b). The elemental mapping along the [100] projected also verified this double kagome lattice at an atomic scale. The false-color image of

elemental mapping of AV_8Sb_{12} (AV_6Sb_6) is shown in Figs. 3(c) and 3(f), from which we can see the atomic arrangements match with the proposed crystal structure shown in Fig. 1.

We use CsV_8Sb_{12} and RbV_6Sb_6 to represent the general behavior of the two newly discovered families. Both the samples exhibit metallic behavior from 300 to 2 K without any anomalies observed [Fig. 4(a)]. We have also measured CsV_8Sb_{12} and CsV_6Sb_6 down to 0.3 K and 100 mK, respectively. No superconductiv-

ity can be observed. The residual-resistance ratios (RRR) are generally low, with the highest value of 2.8 for CsV_8Sb_{12} . Figure 4(b) shows the magnetization of CsV_8Sb_{12} and RbV_6Sb_6 . Both the samples exhibit Pauli magnetism down to 100 K. The upturn at low temperatures may originate from magnetic impurities. Both in and perpendicular to the ab plane, the overall magnetic susceptibility of CsV_8Sb_{12} is nearly four times higher than that of RbV_6Sb_6 .

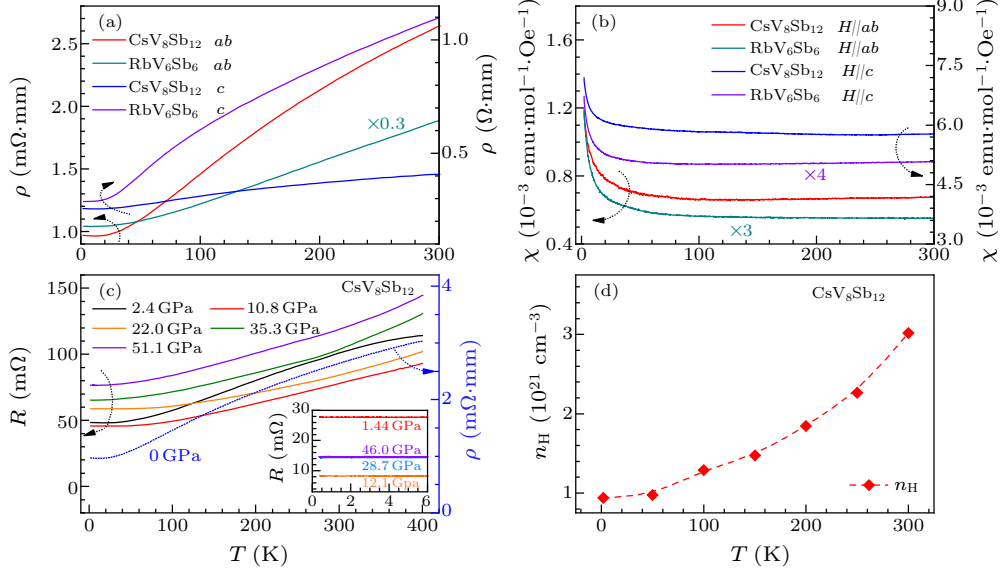


Fig. 4. Electrical transport and magnetization of CsV_8Sb_{12} and RbV_6Sb_6 . [(a), (b)] Temperature-dependent resistivity and magnetization of CsV_8Sb_{12} and RbV_6Sb_6 within the ab plane and along the c -axis. (c) Temperature-dependent resistance of CsV_8Sb_{12} under different external pressure. The measured temperature ranges from 2–400 K. We superimpose the resistivity curve at ambient pressure as the dotted line. Inset: the high-pressure measurements down to 0.3 K. (d) Carrier concentration of CsV_8Sb_{12} against temperature.

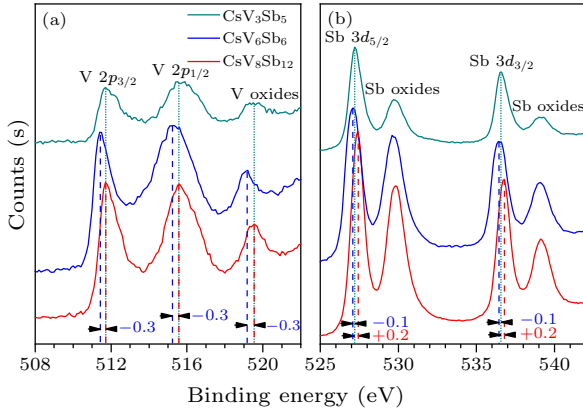


Fig. 5. X-ray photoelectron spectroscopy (XPS) of (a) V 2*p* and (b) Sb 3*d* for CsV_3Sb_5 , CsV_6Sb_6 , and CsV_8Sb_{12} .

The recently discovered reentrance of superconductivity in CsV_3Sb_5 provokes us to further investigate the influence of external pressure on the electric transport properties in AV_8Sb_{12} and AV_6Sb_6 . As shown in Fig. 4(c), the resistance initially decreases from 2.4 to 10.8 GPa. With further increasing the applied pressure, the resistance gradually increases to a high value. We note that the shape

of the RT curve at 2.4 GPa resembles that of resistivity measured at ambient pressure. A prominent feature is the RT curves changing from a convex to concave over 10.8 GPa, indicating a dramatic change of the electrical properties. However, our high-pressure and low-temperature measurements do not show any sign of superconductivity down to 0.3 K [inset in Fig. 4(c)]. Despite the relatively low RRR value found in CsV_8Sb_{12} , the extracted carrier concentration is comparable to that of CsV_3Sb_5 . The Hall coefficient is strongly temperature-dependent, indicating that CsV_8Sb_{12} should be a multi-band system with both hole and electron pockets. Thus, the absence of superconductivity may be closely related to the insertion of the C_2 - V_2Sb_2 layer, which may distort the kagome lattice and alter the pairing mechanism.

The variation of stacking sequence should be directly reflected in the valence state of the investigated elements. To substantiate the influence of the acquired double-layered kagome compounds, we measured the XPS of CsV_3Sb_5 , CsV_6Sb_6 , and CsV_8Sb_{12} , as shown in Fig. 5. The peak positions of Cs are identical for all the three compounds at 723.8 eV, indi-

cating the complete loss of out shell electrons in all the compounds. An interesting discovery is the opposite evolution of V and Sb valence states in CsV_6Sb_6 and $\text{CsV}_8\text{Sb}_{12}$. In CsV_6Sb_6 , the valence state of V $2p$ shifts to lower binding energy, and the peak of Sb $3d$ remains unchanged. Meanwhile, the valence state of V remains intact in $\text{CsV}_8\text{Sb}_{12}$, which is accompanied by the noticeable peak shift of the Sb $3d$ towards higher binding energy. This dramatic difference lies in the fundamental structural difference in their crys-

tal structures. From Fig. 1, the V_3Sb_5 kagome layer is identical in both CsV_3Sb_5 and $\text{CsV}_8\text{Sb}_{12}$, while the building block in CsV_6Sb_6 evolves into V_3Sb_3 with the loss of two Sb atoms on one side. This modification of the kagome layer directly alters the valence state of the V. On the contrary, the inserted building block of V_2Sb_2 in $\text{CsV}_8\text{Sb}_{12}$ connects with the inside V indirectly. Valence modulation of vanadium in the A–V–Sb system through the judicious design of the stacking sequence is realized.

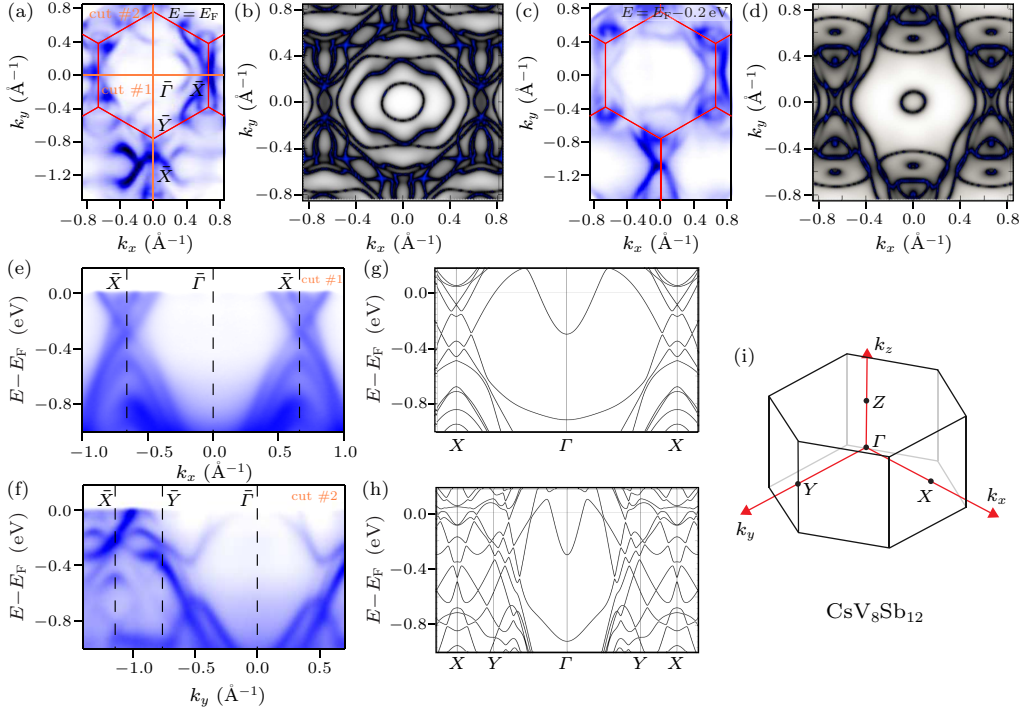


Fig. 6. [(a), (c)] ARPES intensity plots at Fermi surface and constant energy contours at E_F and $E_F - 0.2\text{eV}$ recorded on the (001) surface with $h\nu = 84\text{eV}$. [(b), (d)] DFT calculation at E_F and $E_F - 0.2\text{eV}$. [(e), (f)] ARPES intensity plots showing band dispersions along $\bar{\Gamma}$ – \bar{X} , $\bar{\Gamma}$ – \bar{Y} . [(g), (h)] Calculated band structure along the $\bar{\Gamma}$ – \bar{X} , $\bar{\Gamma}$ – \bar{Y} . (i) Three-dimensional bulk Brillouin zone of $\text{CsV}_8\text{Sb}_{12}$.

To determine the band structure of $\text{CsV}_8\text{Sb}_{12}$, we have carried out systematical ARPES measurements on the (001) cleavage surface of $\text{CsV}_8\text{Sb}_{12}$ single crystal. We summarized constant energy contours and band dispersion in Fig. 6. In-plane Fermi surface (FS) measured with $h\nu = 84\text{eV}$ in Fig. 6(a) clearly shows the C_2 symmetry feature verified in the calculated FS [Fig. 6(b)], and this testifies that the inserted V_2Sb_2 layer has strong modulation on the overall band structure. Constant energy contour [Fig. 6(c)] at 0.2eV below the Fermi level has a good agreement with DFT calculation in Fig. 6(d). We also measured the band dispersion along $\bar{\Gamma}$ – \bar{X} and $\bar{\Gamma}$ – \bar{Y} , as shown in Figs. 6(e) and 6(f), respectively, whose momentum locations are indicated in Fig. 6(a). These results match with our DFT calculations [Figs. 6(g) and 6(h)]. The absence of the electron bands near the Γ point may be caused by the matrix element effect or possible hole-doping of surface Cs loss.

Due to the V_2Sb_2 layer between kagome layers, the point group of $\text{CsV}_8\text{Sb}_{12}$ is D_{2h} , where only a two-fold rotational symmetry persists, in contrast to CsV_3Sb_5 . Near the Fermi level, the states are dominantly attributed to V $3d$ orbitals, from both the kagome V layer and the intercalated V_2Sb_2 layer. The electron-like band around Γ point is attributed to p_z orbitals of Sb atoms in the kagome layer, similar to CsV_3Sb_5 . The two hole bands around Γ point are mainly contributed by the V $3d$ orbitals in the V_2Sb_2 layer. The band at -0.9eV around Γ point is mainly attributed to V d orbitals from both kagome and intercalated layers.

In summary, we have discovered two new families of VSb-based layered compounds, which possess a basic V-kagome lattice similar to that of AV_3Sb_5 . The intercalation of the V_2Sb_2 layer and reorganization of the half- V_3Sb_5 layer lead to a lower symmetry of C_2 ($Cmmm$) and C_3 ($R\bar{3}m$) compared to C_6

($P6/mmm$) of AV_3Sb_5 . The complex of V–V and V–Sb bonding in three-dimensional space increases the diversity of the VSb-based phase. Exertion of thin-flake engineering or chemical substitution may squeeze out more exotic properties like superconductivity and CDW. Furthermore, the frustration of magnetism and non-trivial topological phenomena are also highly expected in more V-kagome-based compounds.

Note: During the preparation of the manuscript, we became aware of two independent works on CsV_6Sb_6 [arXiv:2110.09782] and CsV_8Sb_{12} [arXiv:2110.11452].

References

- [1] Nakatsuji S, Kiyohara N and Higo T 2015 *Nature* **527** 212
- [2] Lin Z, Choi J H, Zhang Q, Qin W, Yi S, Wang P, Li L, Wang Y, Zhang H, Sun Z, Wei L, Zhang S, Guo T, Lu Q, Cho J H, Zeng C and Zhang Z 2018 *Phys. Rev. Lett.* **121** 096401
- [3] Yin J X, Ma W, Cochran T A, Xu X, Zhang S S, Tien H J, Shumiya N, Cheng G, Jiang K, Lian B, Song Z, Chang G, Belopolski I, Multer D, Litskevich M, Cheng Z J, Yang X P, Swidler B, Zhou H, Lin H, Neupert T, Wang Z, Yao N, Chang T R, Jia S and Hasan M Z 2020 *Nature* **583** 533
- [4] Liu E, Sun Y, Kumar N, Muechler L, Sun A, Jiao L, Yang S Y, Liu D, Liang A, Xu Q, Kroder J, Borrmann V S H, Shekhar C, Wang Z, Xi C, Wang W, Schnelle W, Wirth S, Chen Y, Goennenwein S T B and Felser C 2018 *Nat. Phys.* **14** 1125
- [5] Ortiz B R, Gomes L C, Morey J R, Winiarski M, Bordelon M, Mangum J S, Oswald I W H, Rodriguez-Rivera J A, Neilson J R, Wilson S D, Ertekin E, McQueen T M and Toberer E S 2019 *Phys. Rev. Mater.* **3** 094407
- [6] Ortiz B R, Teicher S M L, Hu Y, Zuo J L, Sarte P M, Schueller E C, Abeykoon A M M, Krogstad M J, Rosenkranz S, Osborn R, Seshadri R, Balents L, He J and Wilson S D 2020 *Phys. Rev. Lett.* **125** 247002
- [7] Ni S, Ma S, Zhang Y, Yuan J, Yang H, Lu Z, Wang N, Sun J, Zhao Z, Li D, Liu S, Zhang H, Chen H, Jin K, Cheng J, Yu L, Zhou F, Dong X, Hu J, Gao H J and Zhao Z 2021 *Chin. Phys. Lett.* **38** 057403
- [8] Yin Q, Tu Z, Gong C, Fu Y, Yan S and Lei H 2021 *Chin. Phys. Lett.* **38** 037403
- [9] Jiang Y X, Yin J X, Denner M M, Shumiya N, Ortiz B R, Xu G, Guguchia Z, He J, Hossain M S, Liu X, Ruff J, Kautzsch L, Zhang S S, Chang G, Belopolski I, Zhang Q, Cochran T A, Multer D, Litskevich M, Cheng Z J, Yang X P, Wang Z, Thomale R, Neupert T, Wilson S D and Hasan M Z 2002 *Nat. Mater.* **1**
- [10] Li H, Zhang T T, Yilmaz T, Pai Y Y, Marvinney C E, Said A, Yin Q W, Gong C S, Tu Z J, Vescovo E, Nelson C S, Moore R G, Murakami S, Lei H C, Lee H N, Lawrie B J and Miao H 2021 *Phys. Rev. X* **11** 031050
- [11] Liang Z, Hou X, Zhang F, Ma W, Wu P, Zhang Z, Yu F, Ying J J, Jiang K, Shan L, Wang Z and Chen X H 2021 *Phys. Rev. X* **11** 031026
- [12] Tan H, Liu Y, Wang Z and Yan B 2021 *Phys. Rev. Lett.* **127** 046401
- [13] Chen H, Yang H, Hu B, Zhao Z, Yuan J, Xing Y, Qian G, Huang Z, Li G, Ye Y, Ma S, Ni S, Zhang H, Yin Q, Gong C, Tu Z, Lei H, Tan H, Zhou S, Shen C, Dong X, Yan B, Wang Z and Gao H J 2021 *Nature* **599** 222
- [14] Zhao H, Li H, Ortiz B R, Teicher S M L, Park T, Ye M, Wang Z, Balents L, Wilson S D and Zeljkovic I 2021 *Nature* **599** 216
- [15] Uykur E, Ortiz B R, Wilson S D, Dressel M and Tsirlin A A 2021 arXiv:2103.07912 [cond-mat.str-el]
- [16] Denner M M, Thomale R and Neupert T 2021 arXiv:2103.14045 [cond-mat.str-el]
- [17] Song Y, Ying T, Chen X, Han X, Huang Y, Wu X, Schnyder A P, Guo J G and Chen X 2021 arXiv:2105.09898 [cond-mat.supr-con]
- [18] Chen X, Zhan X, Wang X, Deng J, Liu X B, Chen X, Guo J G and Chen X 2021 *Chin. Phys. Lett.* **38** 057402
- [19] Du F, Luo S, Ortiz B R, Chen Y, Duan W, Zhang D, Lu X, Wilson S D, Song Y and Yuan H 2021 *Phys. Rev. B* **103** L220504
- [20] Yu F H, Ma D H, Zhuo W Z, Liu S Q, Wen X K, Lei B, Ying J J and Chen X H 2021 *Nat. Commun.* **12** 3645
- [21] Chen K Y, Wang N N, Yin Q W, Gu Y H, Jiang K, Tu Z J, Gong C S, Uwatoko Y, Sun J P, Lei H C, Hu J P and Cheng J G 2021 *Phys. Rev. Lett.* **126** 247001
- [22] Wang Q, Kong P, Shi W, Pei C, Wen C, Gao L, Zhao Y, Yin Q, Wu Y, Li G, Lei H, Li J, Chen Y, Yan S and Qi Y 2021 *Adv. Mater.* **33** 2102813
- [23] Yu F H, Wu T, Wang Z Y, Lei B, Zhuo W Z, Ying J J and Chen X H 2021 *Phys. Rev. B* **104** L041103
- [24] Yang S Y, Wang Y, Ortiz B R, Liu D, Gayles J, Derunova E, Gonzalez-Hernandez R, Šmejkal L, Chen Y, Parkin S S P, Wilson S D, Toberer E S, McQueen T and Ali M N 2020 *Sci. Adv.* **6** eabb6003
- [25] Xu H S, Yan Y J, Yin R, Xia W, Fang S, Chen Z, Li Y, Yang W, Guo Y and Feng D L 2021 arXiv:2104.08810 [cond-mat.supr-con]
- [26] Hu Y, Wu X, Ortiz B R, Ju S, Han X, Ma J Z, Plumb N C, Radovic M, Thomale R, Wilson S D, Schnyder A P and Shi M 2021 arXiv:2106.05922 [cond-mat.supr-con]
- [27] Kiesel M L, Platt C and Thomale R 2013 *Phys. Rev. Lett.* **110** 126405
- [28] Wang T, Yu A, Zhang H, Liu Y, Li W, Peng W, Di Z, Jiang D and Mu G 2021 arXiv:2105.07732 [cond-mat.supr-con]
- [29] Song B Q, Kong X M, Xia W, Yin Q W, Tu C P, Zhao C C, Dai D Z, Meng K, Tao Z C, Tu Z J, Gong C S, Lei H C, Guo Y F, Yang X F and Li S Y 2021 arXiv:2105.09248 [cond-mat.supr-con]
- [30] Luo Y, Peng S, Teicher S M L, Huai L, Hu Y, Ortiz B R, Wei Z, Shen J, Ou Z, Wang B, Miao Y, Guo M, Shi M, Wilson S D and He J F 2021 arXiv:2106.01248 [cond-mat.str-el]
- [31] Wu X, Schwemmer T, Müller T, Consiglio A, Sangiovanni G, Di Sante D, Iqbal Y, Hanke W, Schnyder A P, Denner M M, Fischer M H, Neupert T and Thomale R 2021 *Phys. Rev. Lett.* **127** 177001
- [32] Yu J, Xiao K, Yuan Y, Yin Q, Hu Z, Gong C, Guo Y, Tu Z, Lei H, Xue Q K and Li W 2021 arXiv:2109.11286 [cond-mat.supr-con]
- [33] Kresse G and Joubert D 1999 *Phys. Rev. B* **59** 1758
- [34] Kresse G and Furthmüller J 1996 *Comput. Mater. Sci.* **6** 15
- [35] Perdew J P, Burke K and Ernzerhof M 1996 *Phys. Rev. Lett.* **77** 3865
- [36] Monkhorst H J and Pack J D 1976 *Phys. Rev. B* **13** 5188